J Mater Sci (2010) 45:4133–4140
DOI 10.1007/s10853-010-4502-8

Calculation and experimental determinations of the residual stress distribution in alumina/Ni/alumina and alumina/Ni/nickel alloy systems

M. L. Hattali · S. Valette · F. Ropital · N. Mesrati · D. Tréheux

Received: 8 December 2009 / Accepted: 7 April 2010 / Published online: 30 April 2010

Abstract Residual stress problems encountered in joining ceramics–ceramics or ceramics–metals systems for high-temperature applications >1000 °C have been studied. A solid-state bonding technique under hot-pressing via metallic foils sheet of Ni was used for joining alumina–alumina and alumina–nickel alloy (HAYNES® 214™). The residual stresses expected in the specimen were predicted by finite-element method (FEM) calculations using an elastic–plastic-creep model (EPC). Stress distributions in the specimen were characterized experimentally using X-ray diffraction (XRD) and Vickers Indentation Fracture (VIF) techniques. The tensile and shear stress profiles have been determined along selected lines perpendicular to the bonding interface. The results of the FEM calculation of residual stresses have been compared experimentally with the results of classical XRD and indentation methods. It was found that the tensile stress concentration showed higher values at the edge of the boundary. The residual stresses caused by the thermal expansion mismatch between alumina (Al_2O_3) and Ni-based super-alloy (HAYNES® 214™) severely deteriorated the joints compared to Al_2O_3–Al_2O_3 joint with the same solid-state bonding parameters. The correlations between the FEM calculations and experimental results obtained by XRD and VIF method were discussed.

M. L. Hattali (✉) · S. Valette · D. Tréheux
Laboratoire de Tribologie et Dynamique des Systèmes, UMR CNRS ECL ENISE ENSMSE 5513, École Centrale de Lyon, 69134 Ecully Cedex, France
e-mail: hatlam69_2@hotmail.com

S. Valette
e-mail: stephane.valette@ecl-lyon.fr

D. Tréheux
e-mail: daniel.treheux@ecl-lyon.fr

M. L. Hattali · F. Ropital
IFP, BP 3-69360, Solaize, France
e-mail: francois.ropital@ifp.fr

N. Mesrati
Laboratoire de Sciences et Génie des Matériaux, École Nationale Polytechnique d'Alger, 10, Avenue de Hassen Badi EL Harrach, Alger, Algeria
e-mail: n_mesrati@yahoo.fr

Introduction

High-strength ceramic–metal joints are being developed for use in great variety of industrial applications, ranging from structural components in heat engines to coatings in electronic devices [1]. Various techniques for joining ceramic to metal are available, among them the solid-state bonding used in this study [2–7]. However, making a metal–ceramic joint by solid-state bonding method involves inevitably residual stresses as the bonded assembly cools from the joining temperature to room temperature. The magnitude and influence of these shrinkage stresses can be particularly high because of the large difference between the coefficient of thermal expansion (CTEs) and Young's moduli of the three materials and the brittleness of ceramics [8–10]. In some cases, theses residual stresses exceed the bond strength and promote mechanical failure along the ceramic–metal interface. In cases when the bond is strong, the residual stresses tend to cause fracture, generally in the ceramic [11, 12] or ductile in the joint [13, 14].

There is much work available on ceramics/metal joints who were interested to measure strains by diffraction techniques. For example, the residual stresses at the surface of Si_3N_4/carbon steel/Si_3N_4 specimens [15, 16], in vanadium/Al_2O_3 joints [17], or in Al_2O_3/inconel joints [18]

have been studied using conventional X-ray sources. Also, the inner bulk strain field in diffusion-bonded molybdenum/SiC joints [19] and in nickel/Al_2O_3 joints [20] has been determined by neutron diffraction. Other less precise methods were developed such as layer removal techniques [21] and indentation method [22]. These methods makes it possible to determine the level of surface stresses at the point of measurement (tensile stress, compressive stress), and they present a good correlation with measurements taken by X-ray diffraction (XRD) [21]. Additionally, a variety of analytical [23] and numerical models have been developed to understand and optimize the residual stress state in these materials [11, 16, 18, 22, 24]. But rarely they were compared to experimentally measurement with result of classical XRD [16, 18] and indentation fracture method. The most complete comparison was made by Guipont [21]. The agreement is rather good between XRD measurements and FEM estimates. This study is to evaluate the residual stress distribution of two types of bonded specimens, Al_2O_3/Ni/Al_2O_3 and Al_2O_3/Ni/HAYNES® 214, using the XRD measurement and indentation fracture method. Experimental results are compared with predictions obtained using finite-element analysis. A good correlation is found between the FEM calculation and experimental results.

Experimental procedure

Materials

The ceramic material used in the present investigation is a commercial polycrystalline α-Al_2O_3 (AL23 alumina), from UMICORE Marketing services. The ceramic specimens were supplied in the form of 15 × 5 × 5 mm^3 platelets with polished surfaces. The base metal is nickel based super-alloy (HAYNES® 214™) which is used in technological applications at high temperatures and in severe chemical atmosphere. It obtained in the form of rectangular 15 × 5 × 5 mm^3. The filler metal used was a Ni foil 200-μm thick.

The compositions of the used materials are summarized below:

1. Alumina AL23—(>99.7% purity);
2. Nickel—(99.5% purity; 200 μm thick);
3. HAYNES® 214™—Ni super-alloy (75% Ni, 16% Cr, 4.5% Al, 3% Fe).

Prior to bonding, ceramics were polished using diamond pastes to a final grit size of 1 μm. The surfaces of metal interlayer and alloy were lightly polished with silicon carbide abrasive paper in order to remove any oxidation layers. All surfaces were cleaned by immersion in acetone with ultrasonic agitation for 0.5 h. After drying in hot air, the base material blocks and the interlayer foil were prepared as block/foil/block sandwiched assembly, as shown in Fig. 1. Finally, ceramic–metal–alloy "sandwiches" are diffusion bonded by hot-pressing the assembly at 1150 °C. A pressure of 16 MPa through a pneumatic piston was applied to the whole assembly while heating [15, 16]. The heating rate was 150 °C/h and cooling rate was 200 °C/h, and the specimen was held at the maximum temperature for 1 h before cooling to room temperature. The solid-state bonding is carried out in primary dynamic vacuum (10^{-3} Pa) during all the temperature cycle. The experimental conditions were selected taking into account previous studies on alumina/Ni/alumina [5], alumina/Cu/alumina [7], and alumina/Ag/alumina [6] systems.

FEM analysis

In order to estimate the magnitude and distribution of the residual stresses in the joints, FEM calculations were performed. The joining of ceramics and metal is simulated at high temperature (1150 °C). Spatially uniform cooling (i.e., no thermal gradients) and perfect bonding at materials interface were assumed by a quite small cooling rate. FEM analysis was performed using ABAQUS program [25], assuming a two-dimensional geometry under a plane stress-state. To be in agreement with the experimental conditions, the choice of plane stress-state conditions was assumed in FEM analysis because the X-ray penetration is extremely shallow (<10 μm). The stress distribution is then described by principal stresses σ_{xx}, and σ_{yy} in the plane of the surface, with no stress acting perpendicular to the free surface. The actual three-dimensional thermal stresses will affect the plane-stress solution near the interface over a distance comparable to the layer thickness, as has been shown from

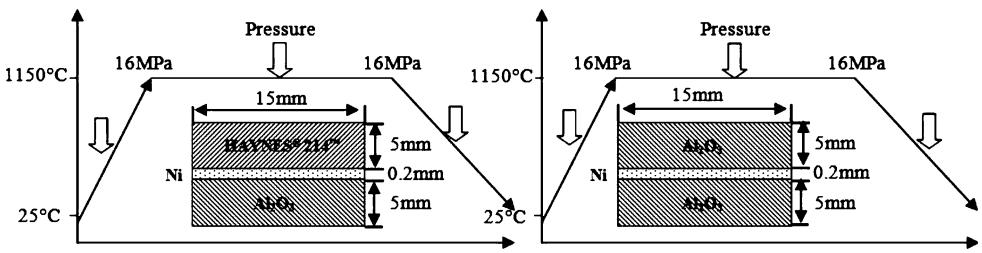

Fig. 1 Schematic drawing of the samples fabricated for the solid-state bonding, and thermal cycle

full three-dimensional elastic calculation of Nakamura [26]. Nevertheless, the plane-stress model accounts for the essential features of elasto-plastic-creep (EPC) deformation [26].

The used conditions and the thermophysical properties for each material are widely described in a previous paper [27] which shows moreover that an EPC calculation was essential to correctly model the Al_2O_3/Ni/HAYNES® 214 system, contrary to the system Al_2O_3/Ni/Al_2O_3 for which an elasto-plastic (EP) calculation was sufficient. In this way, EPC models for the metal and Ni-based super-alloy were adopted. Figure 2 shows the mesh models used in FEM. In ABAQUS, the calculation was accomplished in two parts. The first part concerns a transient heat transfer analysis incorporating the nonlinear thermal conductivity and specific heats of nickel, HAYNES® 214 and alumina as a function of temperature. Subsequently, the resulting temperature distribution as a function of time was incorporated into the thermal stress analysis. The transient heat transfer analysis uses second-order elements of DC2D8 type (eight-node quadratic heat transfer quadrilateral). The transient heat transfer analysis is conducted in three steps. During the first step, the joint is heated to 1150 °C (heating rate was 150 °C/h). During this period, the involved materials are free to expand frictionless. At 1150 °C (step 2), the materials are fixed together. In the third step of the simulation, the joint is cooled down to 25 °C (cooling rate was 200 °C/h). The thermal stress analysis is modeled by second-order eight-node biquadratic plane-stress elements with nine integration points for each element (CPS8R), which, generally, have superior deformation characteristics. The size of the mesh was refined near the intersection of the interface and the free edge of the two materials. Reduced integration elements were used to decrease the analysis cost and to provide more accurate stresses predictions. The thermal stress analysis is also conducted in three steps. In agreement with the experiments, a pressure of 16 MPa was applied all time. Taking advantage of symmetry and using boundary conditions, only a half of the Al_2O_3/Ni/HAYNES® 214 sample had been modeled and a quarter of the Al_2O_3/Ni/Al_2O_3 sample (Fig. 2). In this paper, stress in the *y*-axis, along which the interface of the joint peels or cracks, is mainly discussed because σ_{yy} controls the strength of the joint.

Vickers Indentation Fracture method

The Vickers Indentation Fracture (VIF) method [20, 21] was applied to investigate the residual stresses in the ceramic portion of the bonded joints. A Vickers indenter was impressed at several points in the ceramics at different distances from the interface on the edge of the joint (Line 1—Fig. 2), using a micro-Vickers hardness-testing machine. This method is based on the calculation of the difference between the lengths of cracks observed, induced by indentations for the same ceramic before and after joining (Fig. 3) [20, 21]. In this study, the tests were conducted at a load of 300 g with a loading duration of 15 s every 50 μm, in staggered, from the metal–ceramic interface to ceramic bulk. A Vickers indent may produce two types of cracks, i.e., a system of median cracks and system of Plamqvist cracks. Liang et al. [28] have proposed a universal indentation equation allowing the direct calculation of K_{IC} for both median and Plamqvist cracks. The formula is claimed to the use of any load to perform an indentation test.

$$K_{IC} = \frac{H_V a^{\frac{1}{2}}}{\alpha}\left(\frac{E\varphi}{H_V}\right)^{0,4}\left(\frac{C}{a}\right)^{\frac{C}{18a}-1.51} \quad (1)$$

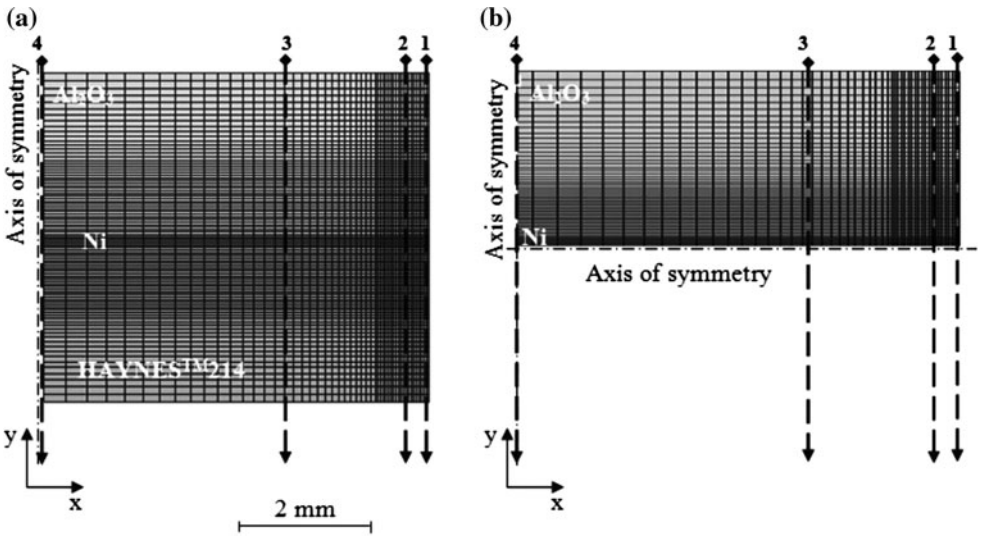

Fig. 2 Geometry of the specimen and the mesh configuration used in the finite-element model. **a** Al_2O_3/Ni/HAYNES® 214™ joint and **b** Al_2O_3/Ni/Al_2O_3 joint. The numbers 1, 2, 3, and 4 represent the lines where residual stresses variation were plotted

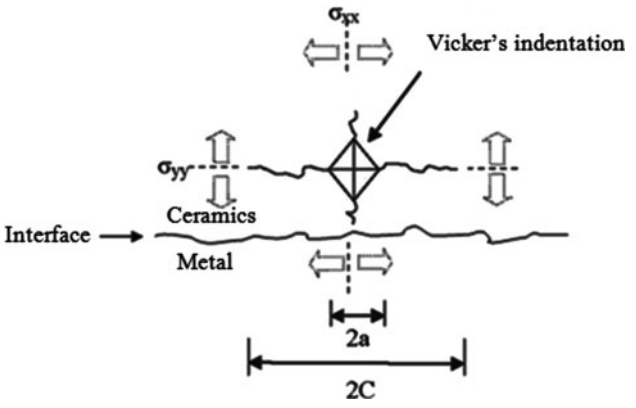

Fig. 3 Indentation fracture method, where 2a is the indent diagonal and 2C is the total length of the radial crack

$$\alpha = 14\left[1 - 8\left(\frac{4v - 0.5}{1 - v}\right)^4\right] \tag{2}$$

where K_{IC} is the fracture toughness, H_v is the Vickers's hardness, v is the Poisson's ratio, φ is a constant close to 3 for alumina, 2a is the indent diagonal, and C is the length of the radial crack (Fig. 3). Lawn and Fuller [29] have suggested a relationship linking the modification of radial crack length to the level of stress σ_s in a surface layer of thickness d taking into consideration the crack pattern produced by a standard point indenter. The residual stress in the ceramic can be calculated using to the following equation:

$$\sigma_r = \frac{K_{IC_i}}{(\pi C\Omega)^{\frac{1}{2}}}\left[1 - \left(\frac{C_i}{C}\right)^{\frac{3}{2}}\right], \tag{3}$$

where K_{IC_i} is the substrate toughness, C_i is the radial crack length before joint, and Ω is a constant depending upon crack geometry $\left(\Omega = \frac{4}{\pi^2}\right)$.

X-ray diffraction method

Because the X-ray penetration is extremely shallow (<10 μm), a condition of plane-stress is assumed. Residual stress measurement was carried out using the $\sin^2 \Psi$ method [30–33] with a Ψ-goniometer (Dosophatex) and INEL software equipments at 30 kV, 30 mA. The size of the collimated X-ray beam (Cr $K_{\alpha 1}$) for residual stress measurement was Ø 800 μm. Measurements were performed with the (300) peak of alumina at $2\Theta = 113°$. The strain (ε) is defined as the relative variation of the actual lattice spacing (d_0), and using the Bragg's equation can be related with the angle shift ($\Delta\theta$) by:

$$\varepsilon = \frac{d - d_0}{d_0} = -\cot\theta X(\Delta\theta) \tag{4}$$

The stress distribution is then described by principal stresses σ_{xx}, and σ_{yy} in the plane of the surface, with no stress acting perpendicular to the free surface. The normal component σ_{zz} and the shear stresses $\sigma_{xz} = \sigma_{zx}$ and $\sigma_{yz} = \sigma_{zy}$ acting out of the plane of the sample surface are zero. A strain component perpendicular to the surface, ε_{zz}, exists as a result of the Poisson's ratio contractions caused by the two principal stresses. The strain in the sample surface at an angle ϕ from the principal stress σ_{xx} in the ceramic can be estimated according to Hooke's law as [34];

$$\varepsilon_{\varphi=0,\psi} = \frac{d_{\varphi=0,\psi} - d_0}{d_0} = \frac{1+v}{E}\sigma_{\varphi=0,\psi}\sin^2\psi - \frac{v}{E}(\sigma_1 + \sigma_2), \tag{5}$$

where $d_{\Phi\,=\,0,\psi}$ is the interplanar spacing of (*hkl*) planes of stressed lattice tilted by ψ and rotated by φ. d_0 is the strain-free lattice interplanar spacing. The terms E and v represent Young's modulus and Poisson's ratio, respectively. σ_1 and σ_2 are the principle stresses. The direction of the diffraction vector was specified by two angles, φ and ψ in the usual way. The d_0 measurements were performed at a fixed value of φ ($\varphi = 0°$) and 21 different values of ψ from −45° to +45° for each φ angle. The Al_2O_3/Ni/Al_2O_3 and Al_2O_3/Ni/HAYNES® 214™ specimens were scanned along two different directions (1 and 4 in Fig. 2) perpendicular to the metal–ceramics interface. Line 1 was at the free end of the specimen, and line 2 was located in the center of the specimen (Fig. 2).

Results and discussion

FEM analysis

The stresses of particular importance are σ_{yy} and τ_{xy}, which govern the modes I and II component of energy release rate. Initially, the assembly is stress-free. During the cooling, the temperature distribution is assumed to be uniform. Figure 4 represents the distribution of the normal stresses σ_{yy} for both Al_2O_3/Ni/HAYNES® 214 and Al_2O_3/Ni/Al_2O_3 assemblies, according to lines indicated in Fig. 2. At the edge of the junction, the stress is strongly in tension (233 MPa, line 1) (Fig. 4a). Tension stress concentration near the specimen edge can cause fracture within the ceramics, in the case of strongly bonded systems, or delamination at the interface for weakly bonded systems. Away from the edge, σ_{yy} tends to decrease, then becomes null (line 4). For the Al_2O_3/Ni/Al_2O_3 system (Fig. 4b), traction is observed only on the free edge (184 MPa, line 1). The maximum of shear stress τ_{xy} is about 65 MPa for Al_2O_3/Ni/HAYNES® 214 joint and 55 MPa for Al_2O_3/Ni/Al_2O_3 joint [35]. The presence of shear stress at the ceramic side near the joint interface, in combination with the tensile stresses that are present, can induce fracturing along

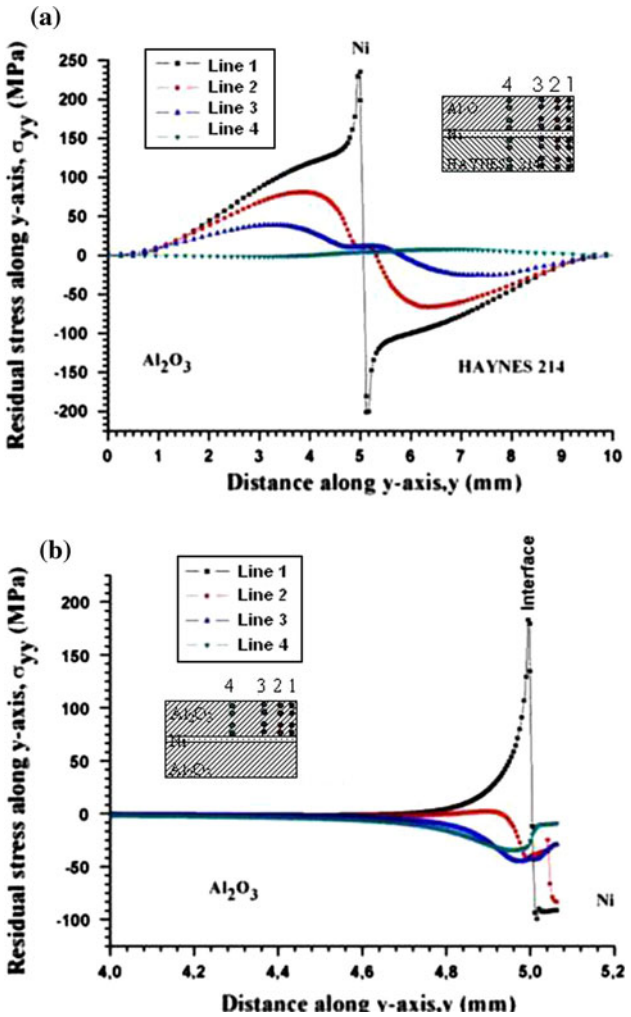

Fig. 4 Normal residual stress (σ_{yy}) profile in the metal/ceramic joint as a function of distance from the interface. This profile is drawn according to the stresses level over an imaginary line (1, 2, 3, and 4) perpendicular to the interface. **a** Al_2O_3/Ni/HAYNES® 214™ joint and **b** Al_2O_3/Ni/Al_2O_3 joint

the ceramic–metal interface. Compressive stress is observed in the nickel layer near the tensile stress concentrated area. In the other area, out of the figure, there was no significant stress or stress distribution.

Vickers Indentation Fracture method

First of all, let us note that measurements of toughness by indentation have advantages, used in this paper (localization of measurement, small samples without machining…) and disadvantages (uncertainties, cracks preceded by a multiplication of dislocations [36]…). Thus, the quantitative comparison with conventional measurements using machined samples (SENB, CVN…) must be considered with prudence. Recently, Quin and Bradt [37] based on information available on the VIF test concluded in their review that the VIF technique is not suitable for the measurement of the fracture toughness K_{IC}. It is necessary to compare the nonconventional VIF technique and Standardized Fracture Toughness tests on the critical points. In particular, for the VIF technique: multiple cracks are generated during the test when the indenter is inserted into the polished specimen surface. In the standard test, loading is applied in universal mechanical testing machine, but the VIF technique the specimen is loaded through a hardness indenter. During loading, in the standard tests, the pre crack extends in a catastrophic manner through the sample. In the VIF method, deformation occurs below and around the indentation; cracks are created and are propagated beneath the indenter, then intersect the surface. The crack slows down, and then stops far from the indenter.

In our study, the aim of K_{IC} measurements by VIF is not to obtain certified value of fracture toughness but to explain some phenomena which cannot be obtained using the standardized fracture toughness tests. Indentation tests were carried out on a cross section of the metal/ceramic interface to see if effects due to interaction between ceramics and metal could be detected.

Figure 5a shows the fracture toughness values of alumina before and after bonding. The variation of fracture toughness of alumina after bonding versus distance from interface was conducted near the free edge (line 1). Fracture toughness values of alumina before bonding were indicated in Fig. 5a. It shows the decrease in ceramic toughness near the interface after solid-state bonding. K_{IC} drops from 7.4 ± 0.4 MPa$\sqrt{\text{m}}$ far from the interface (400 μm), to 3.9 ± 0.35 MPa$\sqrt{\text{m}}$ at 50 μm from the interface. This decrease in toughness already was observed for many metal–ceramics systems and seems to be explained by a weakening effect due to the grain boundary diffusion of the metal in alumina [6]. Indeed, this effect increases with the diffusion time ($K_{IC} = 2.24 \pm 0.1$ MPa$\sqrt{\text{m}}$ was measured after a post-annealing at 900 °C for 120 h). Conversely, the increase in toughness (8.5 MPa$\sqrt{\text{m}}$) observed in the vicinity of 200 μm can be due to a toughening effect by microcracking, there still related to grain boundaries [38, 39], or to the stress field from the surface compression far to the interface (see Fig. 5b) opposing the stress field due to indentation. For a material with residual stresses, the K_{IC} for indentation crack is [40, 41]:

$$K_{IC} = K_{IC}^{\sigma_r=0} + K_{IC}^{\sigma_r}, \quad (6)$$

where $K_{IC}^{\sigma_r=0}$ is the stress intensity factor in a sample with no residual stress, and $K_{IC}^{\sigma_r}$ is the effect due to the residual stress field.

Figure 5b shows that the residual stresses increase from the ceramic bulk (−53 MPa) to metal–ceramics interface (+318 ± 34 MPa). After 120 h post-annealing, the stresses are lower (271 ± 3 MPa).

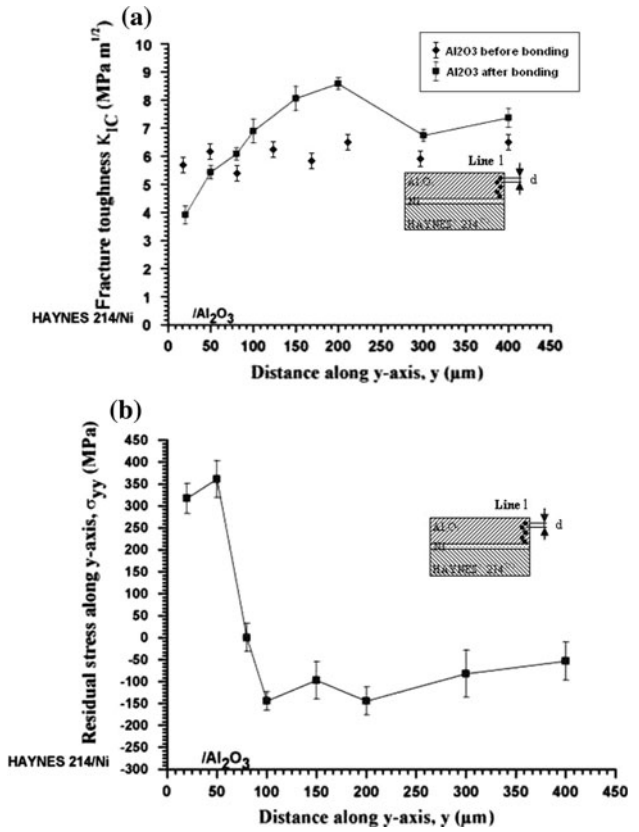

Fig. 5 Evolution of alumina fracture toughness and average residual stress with distance from interface for Al_2O_3/Ni/Haynes®214 joint. **a** Fracture toughness and **b** residual stress. *d* is the distance of the Vickers impression

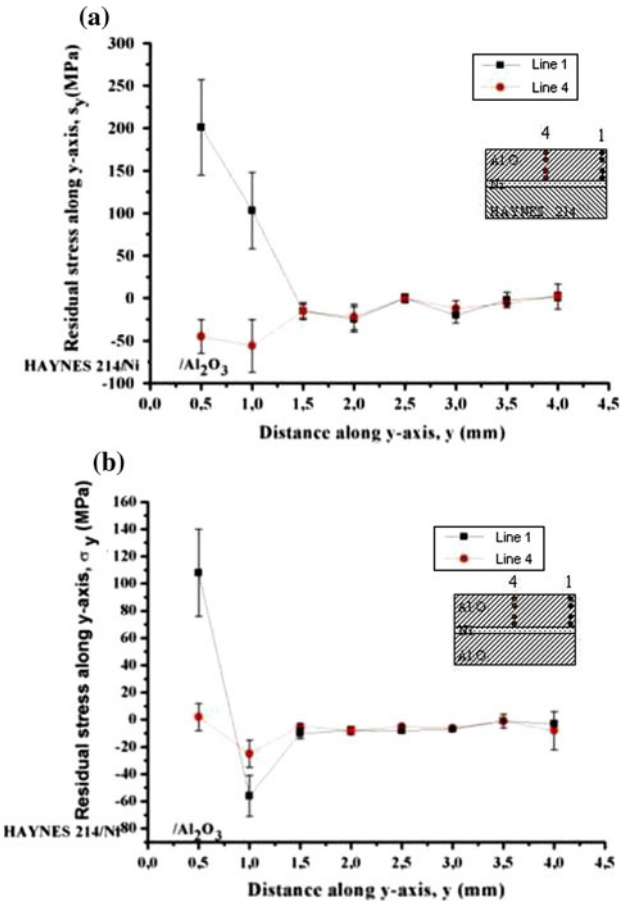

Fig. 6 Tensile residual stress in the ceramic side. **a** Al_2O_3/Ni/Haynes®214 specimen as function of the interfaciale distance for both lines L1 and L2. **b** Al_2O_3/Ni/Al_2O_3 specimen as function of the interfaciale distance for both lines L1 and L2

X-ray stress measurement

Figure 6a, b shows the result of X-ray stress measurement of residual stress distributions, respectively, for Al_2O_3/Ni/Al_2O_3 and Al_2O_3/Ni/HAYNES® 214 joints. For the two systems, it is seen that the level of stress is higher in the direction 1 than the line 4. The stresses were mainly tensile and the maximum was in the vicinity on the Ni/Al_2O_3 interface. After that, the residual stress starts to decrease again and then the residual stress becomes almost constantly null. At the center (line 4), as for FEM analysis, the stresses were compressive near the interface and become negligible in the ceramic bulk. The maximum residual stress of the Al_2O_3/Ni/HAYNES® 214 specimen (201 ± 53 MPa) is higher than that at the Al_2O_3/Ni/Al_2O_3 specimen (108 ± 53 MPa), which confirms again the FEM analysis.

Comparison of methods and crack formation

Figure 7 presents a comparison of the residual stress distributions, in the ceramic close to the interface (line 1), for

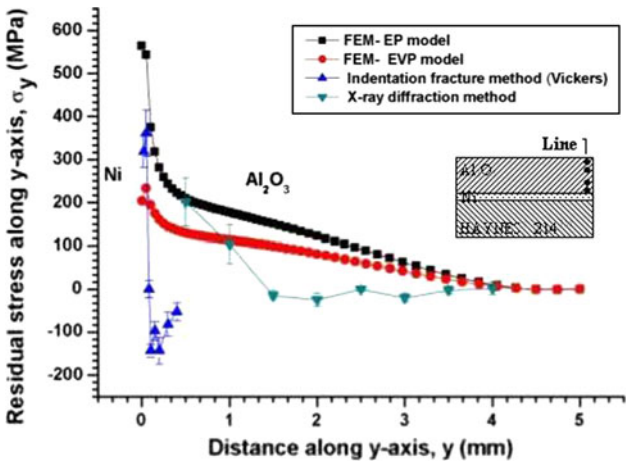

Fig. 7 Comparison of the residual stress distribution obtained by the indentation fracture (IF) method, X-ray method, and finite-element analysis

Al_2O_3/Ni/HAYNES® 214 system, as given by the three different methods (XRD, indentation method, and FEM). The differences between the various methods are not negligible, but the results and the observed differences can, however, be justified.

1. The calculation in EPC, contrary to calculation in EP [27], was essential to modeling ceramic/metal system because EPC results are in good agreement with experimental measurements. The maximum level of stress in the ceramic is found, whatever the method, at the edge of the assembly: 201 ± 53 MPa (X-ray), 318 ± 34 MPa (Indentation method), and 233 MPa (FEM-EVP).
2. XRD measurement underestimates the stresses near by the interface since the first measurements are performed to 0.5 mm of the interface because of the limited practical spatial resolution of the technique (≈800 μm). An extrapolation would give stresses of about 250 MPa, therefore close to the results of FEM and VIF methods. It will be also noted that FEM and XRD profiles are rather close.
3. On the other hand, FEM and XRD measurements do not take account of the modifications of the mechanical properties of alumina in the vicinity of the interface (on 200 μm), probably due to the effect of the nickel diffusion in alumina [6, 27], contrary to the indentation method which clearly highlights these modifications and account holds some. Moreover, this could explain the change of stress sign close to the interface (tension stresses to compressive stresses) in the affected zone. Consequently, the VIF method, which presents the disadvantage of being not very precise, because of the difficulty in determining the lengths of cracks, but has the advantages of permitting measurement close to the interface.

In any case, the presence of shear stress at the ceramic side, near the joint interface, in combination with the tensile stresses that are present, may cause cracks in the joint, or failure of bonding. Indeed, through fractographic analysis of specimens, it is found that the crack initiates at the edge of the interlayer and then changes its direction into the ceramic and propagates into the ceramic part near the interface [27]. This phenomenon is observed only in dissimilar Al_2O_3/Ni/HAYNES® 214 bonds. It is in accordance with FEM analysis, and XRD or VIF measurement.

Conclusions

The residual stress distribution in symmetrical Al_2O_3/Ni/Al_2O_3 and dissimilar Al_2O_3/Ni/HAYNES® 214 bonds have been characterized using the XRD method, the indentation fracture method, and was also calculated using the finite-element method. Based on the results obtained in this work, the following conclusions can be drawn.

1. The results of the three employed methods show that the highest tensile stress is concentrated at the boundary of the outer surface of the joint, and it will cause cracks in alumina layer only in the case of dissimilar Al_2O_3/Ni/HAYNES® 214 bonds.
2. The maximum residual tensile stress of Al_2O_3/Ni/Al_2O_3 specimen was lower than that of the Al_2O_3/Ni/HAYNES® 214 specimen.
3. The results obtained by FEM analysis, X-ray, and VIF measurements show the same trend of stress distribution and the highest tensile stress concentration at the outer surface of the boundary of the joint. The FEM and X-ray results are in rather good agreement, knowing that certain phenomena, such as grain boundary diffusion of nickel in alumina, are not taken into account. The indentation method tends to overestimate the stresses, probably taking into account the fall of toughness of ceramics close to the interface.
4. FEM is an effective method to predict the stress distribution in symmetrical Al_2O_3/Ni/Al_2O_3 and dissimilar Al_2O_3/Ni/HAYNES® 214 bonds. The result at the FEM simulation shows that the filler metals zone and the base materials part adjacent to this zone are the high-residual stress concentration. These results explain very well the fractography observation of the Al_2O_3/Ni/HAYNES®214 joints [27].

References

1. Larson DS, Adams JW, Johnson LR, Teotia APS, Hill LG (1985) Ceramic materials for advanced heat engines. Noyes, Park Ridge, NJ
2. Lino Y (1990) J Mater Sci Lett 10:104
3. Nicholas MG (1990) Joining of ceramics. Chapman & Hall, London
4. Das S, Tiwari AN, Kulkarni AR (2004) J Mater Sci 39:3355. doi: 10.1023/B:JMSC.0000026935.18466.4b
5. Lourdin P, Juvé D, Tréheux D (1996) J Eur Ceram Soc 16(7):745
6. Serier B, Tréheux D (1993) Acta Metall Mater 41(12):369
7. Kara-Slimane A, Mbongo B, Tréheux D (1999) J Adhesion Sci Technol 13:35
8. Esposito L, Bellosi A, Guicciardi S, De portu G (1998) J Mater Sci 33:1827. doi:10.1023/A:1004397019927
9. Evans A, Dalgleish B, Hutchinson J (1989) Acta Metall 37:3249
10. Hsueh C, Evans A (1999) J Eur Ceram Soc 13(1):35–48
11. Zhang JX, Chandel YZ, Seow HP (2002) J Mater Proc Tech 122:220
12. Cao H, Evans A (1989) Mech Mater 7:295–304
13. Dalgleish B, Trumble K, Evans A (1989) Acta Metall 37(7): 1923–1991
14. Drory M, Evans A (1990) J Am Ceram Soc 73:634
15. Lee SB, Kim JH (1997) J Mater Process Technol 67:167

16. Kurita M, Sato M, Ihara I (1977) J Am Ceram Soc 86:60
17. Nemoto Y, Ueda K, Satou M, Hasegawa A, Abe K (1998) J Nucl Mater 163:1517
18. Colin C (1991) Détermination des contraintes résiduelles dans les assemblages alumine/Inconnel 600, Thèse de l'Ecole des mines de Paris
19. Martinelli AE, Drew RAL, Fancello EA, Rogge R, Root JH (1999) J Am Ceram Soc 82:1787
20. Rabin BH (1998) J Am Ceram Soc 81:1541
21. Tréheux D, Fayeulle S, Guipont V, Jacquemin JP (1998) In: Bellosi A et al (eds) Interfacial science in ceramic joining. Kluwer Academic Publishers, New York, p 311–318
22. Lascar G (1998) J Phys IV 4:115
23. Iancu OT, Munz D, Eienmann B, Scholtes B, Macherauch E (1990) J Am Ceram Soc 73(5):1144–1149
24. Travessa DN, Ferrante M, Den Ouden G (2000) Mater Sci Technol 16:687
25. ABAQUS Software (2006) User's manual, version 6.6. Karlsson and Sorensen Inc, Hibbitt
26. Nakamura T (1991) ASME J Appl Mech 58:939
27. Hattali ML, Valette S, Ropital F, Mesrati N, Tréheux D (2009) J Mater Sci 44:3198. doi:10.1007/s10853-009-3426-7
28. Liang KM, Orange G, Fantozzi G (1990) J Mater Sci 25:207. doi:10.1007/BF00544209
29. Lawn BR, Fuller ER Jr (1984) J Mater Sci 19:4061. doi:10.1007/BF00980772
30. Maeder G (1989) Chem Scrip 26A:23–31
31. ASTM Book of standards Volume: 03.01,CS03. A standard method for verifying the alignement of X-ray diffraction instrumentation for residual stress measurement. ASTM International, West Conshohocken, PA (2002)
32. ASTM Book of standards Volume: 03.01. A standard test method for determining the effective elastic parameter for X-ray diffraction measurements of residual stress. ASTM International, West Conshohocken, PA (2009)
33. Hattali L (2009) Carcatérisation et modélisation Thermo-mécaniques des assemblages métal-céramique élaborés par thermocompression, Thèse Ecole Centrale de Lyon N 2009-02
34. Noyan IC, Cohen JB (1987) Residual stress, measurement by diffraction and interpretation, Materials Research Engineering. Springer-Verlag, New York
35. Hattali ML, Valette S, Ropital F, Mesrati N, Tréheux D (2009) IOP Conf Series Mater Sci Eng 5:012011. doi:10.1088/1757-899X/5/1/012011
36. Hockey BJ (1971) J Am Ceram Soc 54(5):223
37. Quinn GD, Bradt RC (2007) On the Vickers indentation fracture toughness test. J Am Ceram Soc 90(3):673
38. Simpson LA, Ritchie IG, Lloyd DJ (1975) J Am Ceram Soc 58(11–12):537
39. Noone MJ, Mehan RL (1973) In: Bradt RC, Hasselman DPH, Lange FF (eds) Fracture mechanics of ceramics, vol 1, Plenum, New York
40. Marshall DB, Lawn BR (1977) J Am Ceram Soc 86(1):60
41. Simpson LA (1973) J Am Ceram Soc 56:7–11